NANO LETTERS

2001
Vol. 1, No. 12
697−702

Molecular Dynamics Simulation of Contact Angles of Water Droplets in Carbon Nanotubes

Thomas Werder,*,† Jens H. Walther,† Richard L. Jaffe,‡ Timur Halicioglu,§ Flavio Noca,|| and Petros Koumoutsakos†,⊥

Institute of Computational Science, ETH Zurich, Weinbergstr. 43, CH-8092, Switzerland, NASA Ames Research Center, Moffett Field, California 94035, Eloret Corporation, 690 W. Fremont Avenue, Sunnyvale, California 94086, and Jet Propulsion Laboratory, 4800 Oak Grove Drive, Pasadena, California 91109

Received October 3, 2001; Revised Manuscript Received October 20, 2001

ABSTRACT

We study the behavior of water droplets confined in a carbon nanotube by means of parallel molecular dynamics simulations. We report radial density profiles, radial hydrogen bond distributions, and contact angles for tube radii ranging from 12.5 to 37.5 Å and for droplets containing up to 4632 water molecules. Our results indicate nonwetting behavior of the pristine CNT at room temperatures.

Introduction. Since the discovery of carbon nanotubes (CNT) by Iijima,[1] the field of prospective applications continues to expand. A particular area of interest is the use of carbon nanotubes in nanofluidics applications. Nanofluidics is the study of fluid (gas, liquid) flow around and inside nanoscale systems. Nanofluidics is envisioned as a key technology for designing engineering devices for biological applications, such as biomedical devices (e.g., nanoexplorers, cell manipulators, etc.) in which the dominant biomolecular transport process is carried out by natural and forced convection. Other applications include the usage of CNT as nanopipets,[2] as sieves for DNA sequencing applications, and (in arrays of carbon nanotubes) as acoustic sensors in the form of artificial stereocilia.[3] As a starting point for these applications, we have been studying the canonical problem of the interaction of water with carbon nanotubes, and in particular in this paper we consider the behavior of water droplets confined in carbon nanotubes. A fundamental issue is the ability of a fluid to wet the interior of a CNT as this would facilitate solution chemistry inside CNT.[4] Dujardin et al.[5] found experimentally that liquids with surface tension exceeding the limit of approximately 130−170 mN/m do not wet single-wall CNT (SWNT) bundles. According to these arguments water should wet CNT, as the surface tension of water at room temperature is 72 mN/m. However, the purity of the nanotube samples and the chemical composition of the liquid samples were not specified. Gogotsi et al.[6,7] observed wetting of CNT by aqueous inclusions formed during the process of hydrothermal synthesis of multiwall CNT. In these experiments the estimated composition of the fluid inclusion is 85.2% water, 7.4% CO_2, and 7.4% CH_4, which may exhibit different behavior from pure water inside a pristine SWNT. In a related study of water droplets on a flat graphite surface under high relative humidity, Luna et al.[8,9] measured the contact angle of water on graphite to be 30°, which is indicative of pronounced wetting. However, they state that minuscule amounts of impurities could drastically influence their measurements. They also report observation of a 5-nm thick mobile water layer that slowly transforms into a 2-nm thick ice-like layer. This apparent wetting of CNT and graphite by water is contrasted by the general notion that the surface of graphite is hydrophobic, that the contact angle of water on graphite is 80−90°,[10] and that CNTs have a low solubility in water.[11] However, it should be noted that the measured contact angle of liquid drops on a smooth surface appears to decrease as the size of the drop decreases (see Rieutord and Salmeron[12]).

The intrinsic difficulties in experimental characterization of thermodynamic and structural properties of nanoscale structures have motivated the extensive use of computational techniques such as molecular dynamics simulations (MD). Recently, Gordillo and Martí[13] conducted numerical simulations of SWNTs completely filled with water. In particular, they find that for SWNTs with diameters in the range between 8.2 Å and 16.3 Å, the hydrogen bond network of the water is distorted due to the confinement of the water.

* Corresponding author. E-mail: werder@inf.ethz.ch.
† Institute of Computational Science, ETH Zurich.
‡ NASA Ames Research Center.
§ Eloret Corporation.
|| Jet Propulsion Laboratory.
⊥ Also at Center for Turbulence Research, NASA Ames/Stanford University.

10.1021/nl015640u CCC: $20.00
Published on Web 11/10/2001

Table 1: Overview of the CNT−Water Systems[a]

case	chirality	D^b [Å]	$N_{H_2O}{}^c$	$N_C{}^d$	type[e]	$\epsilon_{CO}{}^f$ [kJ mol^{-1}]
A	(32, 0)	25.0	360	4224	flexible	0.3135
B	(64, 0)	50.0	1872	8448	flexible	0.3135
B^0	(64, 0)	50.0	1872	8448	rigid	0.3135
B^0_+	(64, 0)	50.0	1872	8448	rigid	0.3762
B^0_-	(64, 0)	50.0	1872	8448	rigid	0.2508
C	(96, 0)	75.0	4632	12672	flexible	0.3135
G_1	graphite 1L	∞	1210	576	flexible	0.3135
G_2	graphite 2L	∞	1210	1152	flexible	0.3135
G_2^0	graphite 2L	∞	1210	1152	rigid	0.3135

[a] All systems are periodic in the direction of the tube axis. The length of the tubes is 138.9 Å and the chirality corresponds to a zig-zag CNT.[b] D denotes the diameter of the CNT. [c] N_{H_2O} is the number of water molecules. [d] N_C is the number of carbon atoms in one periodic image of the system. [e] Flexible and rigid refer to the force field description of the CNT. [f] The Lennard-Jones parameter ϵ_{CO} determines the interaction strength between the water and the graphite. The cases B^0_+ and B^0_- have a 20% larger and lower value for ϵ_{CO}, respectively, than the reference values. Case G_i refers to the simulation of the planar graphite−water system, and i indicates the number of graphite layers.

The impurities encountered in experiments (e.g., presence of amorphous carbon and catalyst particles on the CNT surface and ions and other liquid contaminants in the water) can change the wetting behavior. On the other hand, the behavior exhibited in MD simulations of pure components is subject to the uncertainties in the choice of parameters for the interaction potentials. In this letter we focus on wetting aspects and on structural properties of water droplets confined in SWNT using large scale parallel MD simulations. We examine the equilibrium shape of the water droplet and deduce its contact angle with the CNT surface. This is done using isochore line plots of the water following the algorithm suggested by Nijmeijer.[14] Additionally, radial water density profiles and radial hydrogen bond distributions are reported. The systems considered include zigzag CNTs with diameters of 25.0, 50.0, and 75.0 Å respectively and initially flat 23.7 Å thick drops (this corresponds to 12 layers of water molecules), see the overview in Table 1. The simulations indicate that pure water does not wet pristine single wall carbon nanotubes.

Methodology. We implement parallel molecular dynamics (MD) simulations. The MD simulations are based on the following force field: (i) The *water−water* interaction is modeled by a flexible SPC water model[15] that accounts for intramolecular degrees of freedom including harmonic O−H bond potentials and a H−O−H angle potential. The intermolecular interactions consist of an O−O Lennard-Jones potential and a Coulomb potential between point charges residing on the atoms. (ii) The *valence force field* for the CNT includes a Morse potential, harmonic angle potential, and a torsion potential.[16] A C−C Lennard-Jones interaction is added with the standard 1-2 and 1-3 nearest neighbor exclusion rules applied. (iii) The *carbon−water* interaction consists of a Lennard-Jones term between the carbon and oxygen atoms where the parameters of the potential, $\epsilon_{CO} = 0.3135$ kJ mol^{-1} and $\sigma_{CO} = 3.19$ Å, are obtained from the experimental data of Bojan and Steele.[17]

The nonbonded interactions (including van der Waals and Coulomb potentials) are both considered within a cutoff distance r_c of 10 Å using smooth truncation of the potentials.[18] For a complete description of the potential models and parameters used in the present study, we refer to the work of Walther et al.[16] and the references therein. The electrostatic energy term between the carbon atom quadrupole moments and the water partial charges is not included in this work.

The equations of motion are integrated using a leapfrog scheme with a time step of 0.2 fs. Periodic boundary conditions are imposed in the direction parallel to the tube axis, and free space conditions prevail in the normal directions. The length of the CNT is 138.9 Å. During the first 4 ps of equilibration (total equilibration time is 30 ps), the system is coupled to a Berendsen thermostat[19] at a temperature of 300 K. In the second part of the equilibration and for the sampling, the thermostat is turned off and the system is allowed to evolve according to the force field described earlier. In all cases, statistics are collected during the remaining 170 ps and samples are taken every 0.04 ps.

The present parallel implementation is based on a spatial domain decomposition method using the message passing interface (MPI). The bonded interactions are handled by maintaining a global bond list that is shared by all processors and which allows all processors to extract the local information needed while the non bonded interactions are treated with a standard ghost layer approach. A single time step of the largest system considered in this study (case C with 4632 water molecules and 12672 carbon atoms, see below) requires 0.56 s on a Linux Beowulf cluster using 8 Pentium III/500 MHz processors (100 MBit/s UTP Ethernet) and 2.93 s on a single processor, corresponding to a speed-up of 5.2.

Results and Discussion. The present study considers nanometer-size droplets of water in carbon nanotubes of diameters 25.0 Å, 50.0 Å, and 75.0 Å respectively (the cases A, B, and C). Twelve layers of randomly oriented water molecules form the initially flat drops. The spacing of the water molecules on a cubic lattice is chosen such that the initial water density amounts to 1 g cm^{-3}. The cases B^0, B^0_+, and B^0_- have identical initial configurations as case B, but the zero superscript signifies that the carbon nanotube is "rigid", i.e., that the position of the carbon atoms is fixed during the simulation. Thus, the influence of the CNT on the droplet shape is limited to the Lennard-Jones interaction, which is controlled by the parameters ϵ_{CO} and σ_{CO}. In case B^0, the reference value of $\epsilon_0 = 0.3135$ kJ mol^{-1} is used, while this value is increased by 20% for case B^0_+ and lowered by 20% for case B^0_- (σ_{CO} is 3.19 Å in all cases).

The cases G_1, G_2, and G_2^0 involve a slab of water covering a planar graphite sheet where the zero superscript again denotes "rigid" graphite atoms and the subscript encodes the number of graphite layers. The size of the computational domain is 39 × 39 × 100 Å, and periodic boundary conditions are imposed in all spatial directions. The water slab is initially 10 molecules thick. The overall simulation length is 200 ps for the cases A, B, and C and 100 ps for the cases B^0, B^0_+, B^0_-, G_1, G_2, and G_2^0. A summary of these systems is given in Table 1.

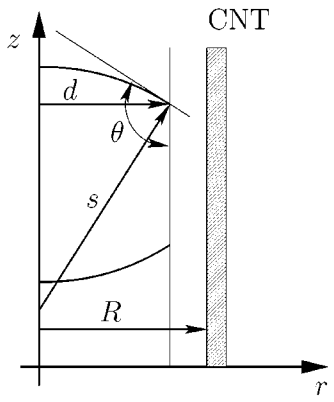

Figure 1. Schematic of the CNT−water system. R denotes the tube radius and z the tube axis. The contact angle θ is determined from the radii d and s by the relation $\theta = \pi - \cos^{-1}(d/s)$, where d is an inner radius that excludes the near wall water layering and s is the radius of the fitted sphere.

The radial density and hydrogen bond distributions are measured in the central part of the drop using 50 radial bins of constant volume for case A and 100 and 150 bins, respectively, for cases B and C. This binning is centered vertically at the center of mass of the drop, and the height of the bins is 19.8 Å in all cases. For the calculation of the water isochore profiles, a total of 250 bins is used along the z axis while the resolution in the radial direction is similar to that used for the radial profiles. The resulting bin spacing along z is 0.56 Å and the bin volume is 5.5, 11, and 16 Å^3 for cases A, B, and C, respectively. All quantities that are plotted for the CNT−water cases are averaged circumferentially and are displayed as a function of the radius r. A schematic of the CNT−water systems is shown in Figure 1.

The water radial density profiles for the three different diameter tubes are shown in Figure 2a and 2b. Note that the r axis corresponds to the distance from the CNT wall toward the center of the tube. Using a standard sampling technique (Figure 2a), the density profiles display an apparent reduction of the density peaks for the large diameter CNTs and a shift of position of the peaks toward the center of the tubes. However, this significant reduction of the peaks is partially an artifact of the binning as demonstrated in Figure 2c, where a conditional binning has been applied. The CNTs are modeled by a force field that accurately reflects their mechanical behavior, e.g., it is able to reproduce the correct vibrational modes of the CNT as reported in ref 16. Thus, the CNT does not retain the initial cylindrical shape that is assumed for the standard circumferential averaging. This leads to a smearing of the radial density peaks since the binning, as applied to a CNT with an ellipsoidal cross section, spreads the near-wall water molecules over more bins than it would for a CNT with a circular cross section. A straightforward way to circumvent this problem is to use a conditional binning, where a sample is accepted when the standard deviation of the C atom positions from the cylindrical shape is less than 0.4 Å. This threshold was determined by inspection of the evolution of the CNT cross sections in time. Using the conditional binning, 88.8% of the samples for case B and 26.3% of the samples for case C are accepted. The cases where a conditional binning is applied are marked with a prime. The comparatively small tube in case A is not affected by the conditional binning, since it fulfills the regularity criterion for every sample. As illustrated in Figure 2b, the lowering and shifting of the peaks is largely reduced. The remaining differences are attributed to curvature effects;

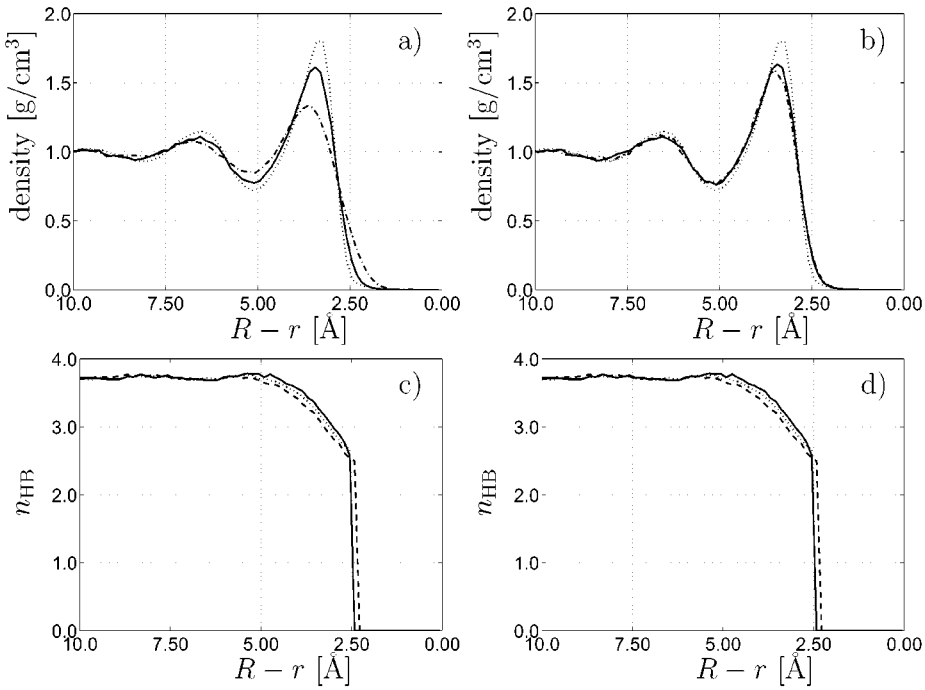

Figure 2. Water radial density profiles and hydrogen bond profiles of a water drop inside a carbon nanotube are presented. All profiles are measured at the center of the drop, but while in (a) and (c) a standard sampling technique is applied (cases A, B, and C), we used a conditional binning in (b) and (c) (cases A, B′, and C′). The tube diameters are 25.0 (···), 50.0 (—), and 75.0 Å (-·-), and R denotes the radius of the individual tubes.

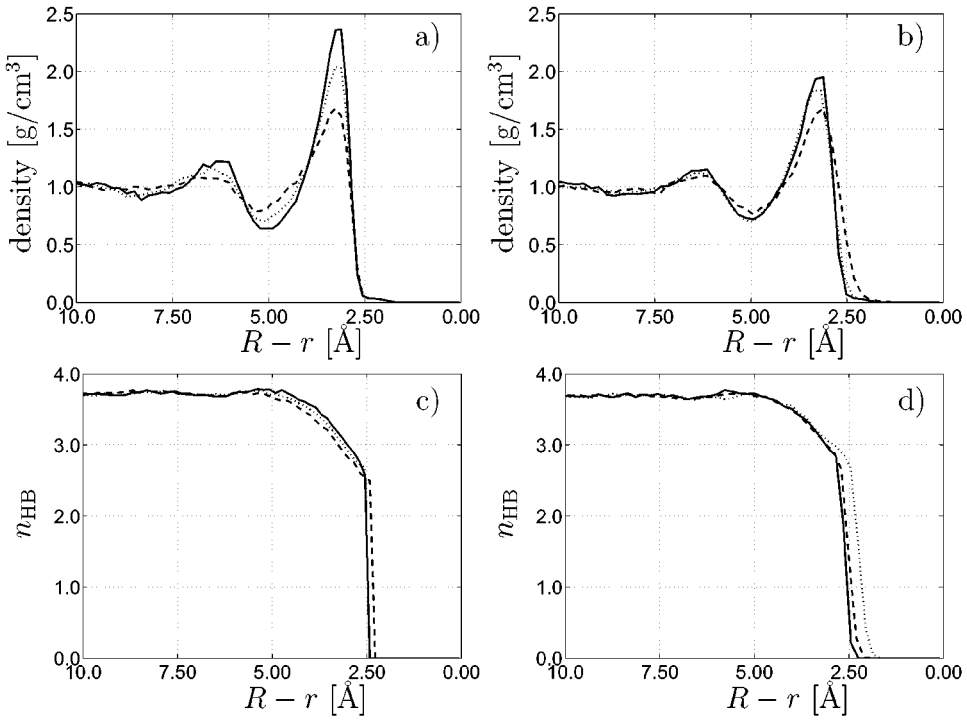

Figure 3. Water radial density profiles and hydrogen bond profiles are presented for a water drop inside a carbon nanotube (a, c) and for a water layer on graphite (b, d). The profiles in (a) and (c) are from the cases B^0 (···), B^0_+ (—), and B^0_- (− −), which denote the same water−CNT geometry but have a different water−CNT Lennard-Jones interaction strengths. The reference value of $\epsilon_{CO} = 0.3135$ kJ mol^{-1} for case B^0 is increased by 20% in case B^0_+ and lowered by 20% in case B^0_-. Figures (b) and (d) display analogous plots for the graphite cases, which include a single flexible layer in case G_1 (− −), a double flexible layer in case G_2 (···), and a double rigid layer in case G^0_2 (—).

in other words, a water molecule in a small diameter CNT is subject to an increased influence from the wall and to a reduction of the intermolecular water interaction.

The hydrogen bond distributions shown in Figures 2 and 3 are found using the geometrical definition of Martí,[20] which assumes that two water molecules are hydrogen bonded if (i) the oxygen−oxygen distance is smaller than 3.6 Å, (ii) the distance between the oxygen of the donor and the hydrogen of the acceptor is less than 2.4 Å, and (iii) the bond angle between the O−O direction and the molecular O−H direction of the donor, where H is the hydrogen that forms the bond, is less than 30°. In Figure 2c the plots are generated using all samples, while in Figure 2d only the samples that fulfill the conditional sampling criterion are used. In both cases the number of hydrogen bonds amounts to approximately 3.7 in the central part of the drop, which corresponds to the value for bulk water. It can be observed that the number of hydrogen bonds decreases more slowly near the wall for the larger diameter CNTs, reflecting the fact that water molecules have fewer neighbors close to a strongly curved wall. A molecule in the outermost water layer forms on average approximately 2.6 hydrogen bonds.

To study the role of the water−carbon interaction, three additional cases (B^0, B^0_+, and B^0_-) were studied for systems with rigid walls. The Lennard-Jones potential well depth (between an oxygen and a carbon atom) was increased or reduced by 20% from the reference value, corresponding to $\epsilon_{CO} = 0.3135$ kJ mol^{-1}, $\epsilon^+_{CO} = 0.3762$ kJ mol^{-1}, $\epsilon^-_{CO} = 0.2508$ kJ mol^{-1} for the cases B^0, B^0_+, and B^0_-, respectively. In Figure 3, the rigid cases B^0, B^0_+, and B^0_- are compared. The differences induced by the variation of the interaction strength manifest themselves in the peak height and also in the value of the contact angle, as will be seen later. The higher the value of the parameter ϵ_{CO}, i.e., the stronger the water−carbon interaction, the higher the peak. The hydrogen bond number and distribution are only slightly affected by the difference in the interaction strength, supporting the conjecture that these properties are governed by confinement effects. The cases with the water slab on graphite (G_1, G_2, and G^0_2) are the limiting case of a CNT−water system where the CNT has an infinite radius. In that sense, the double-layer graphite cases might be perceived as models for multiwall CNTs. The double layer cases G_2 and G^0_2 exhibit higher peaks in the radial density functions than the single layer case G_1, see Figure 3b, due to the increased van der Waals attraction between the water and the graphite.

The notion of a contact angle in its classical meaning is a macroscopic concept that is not fully applicable on the nanometer scale.[21] Nevertheless, Nijmeijer et al.[14] suggested a technique to visually determine the contact angle of a fluid between two walls, which is based on the observation that the liquid−vapor interface would relax to a spherical shape. Following their work, we measure the contact angle by fitting a circle to the isochore lines of 0.45, 0.55, 0.65, and 0.75 g cm^{-3} using a least-squares method, see Figure 1. In this procedure, we neglect the first 7.5 Å in radius of the water

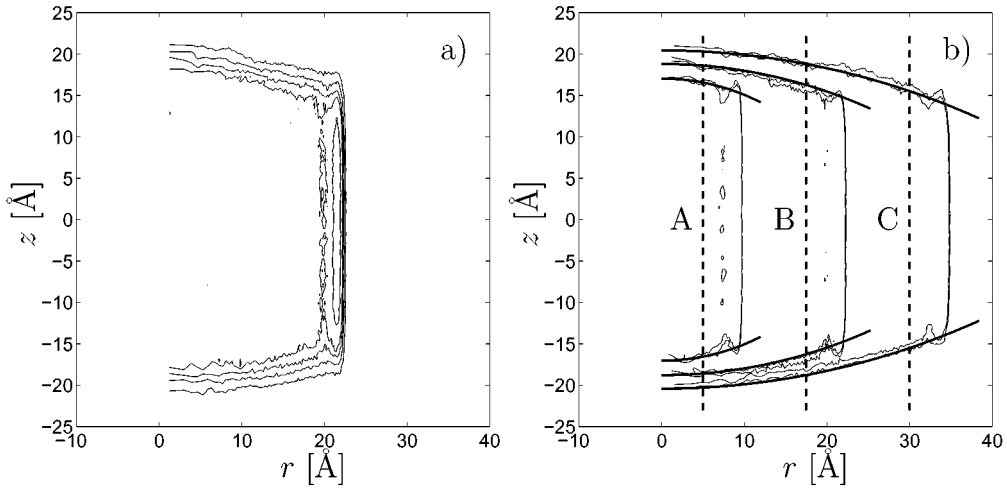

Figure 4. Determination of the contact angle. (a) Isochore line plot for case B at the levels 0.2, 0.4, 0.6, 0.8, and 1.0 g cm^{-3}, respectively. (b) Plot of the isochore lines 0.6 and 0.7 g cm^{-3} for the cases A, B, and C. The least squares fit of the 0.65 g cm^{-3} isochore line is superposed. For the fit, only the part of the isochore lines that lies outside the CNT−water interface is considered (indicated by the vertical lines).

Table 2: Computed Contact Angles for Tubes of Different Diameters: 25 Å (case A), 50 Å (case B) and 75 Å (case C)[a]

	isochore [g cm^{-3}]				
case	0.45	0.55	0.65	0.75	error
A	103.0°	103.0°	100.9°	106.2°	±4.8°
B	104.4°	105.2°	106.4°	107.6°	±0.9°
B′	104.3°	104.9°	105.8°	107.0°	±0.6°
B^0	105.3°	107.2°	109.9°	115.4°	±1.1°
B$^0_+$	102.6°	103.8°	105.0°	107.7°	±1.5°
B$^0_-$	125.3°	129.2°	132.2°	136.4°	±2.6°
C	105.3°	106.1°	107.2°	109.1°	±0.3°
C′	104.4°	105.3°	106.2°	107.9°	±0.4

[a] Cases B′ and C′ denote the results obtained using the conditional binning. Cases B^0, B$^0_+$, and B$^0_-$ involve fixed CNTs with the reference (cases B^0) and perturbed (cases B$^0_+$ and B$^0_-$) Lennard-Jones parameters. The angles are obtained by fitting a sphere through isochore surfaces of the water meniscus. The conditional binning has a negligible influence on the contact angle for case A, it reduces the number of samples for B and C to 89% and 26%, respectively. The errors are the maximum errors (for each row) as computed from the standard deviation of the fit.

meniscus from the wall, as indicated by the dashed vertical lines in Figure 4b. This effectively excludes the large density variations that do not contribute to the macroscopic contact angle. The 0.6 and 0.7 g cm^{-3} isochore lines for the cases A, B, and C are shown in Figure 4b with the circular curves superimposed that fit the at 0.65 g cm^{-3} isochore. An inspection of the isochores in Figure 4 reveals that a variation of the size of the exclusion zone in a range from 5 to 10 Å would not affect the value of the contact angle significantly. As an example, the complete water isochore contours for the levels 0.2, 0.4, 0.6, 0.8, and 1.0 g cm^{-3} for case B are shown in Figure 4a. The values obtained for the contact angle are given in Table 2. The error estimates are the maximum standard deviation of the four least squares fits in each row. The results clearly indicate that none of the systems exhibit wetting and that the smallest contact angle, 103°, is found for the smallest-diameter tube considered (case A). This is in reasonable agreement with the macroscopic value measured for water on graphite (a value of 80−90° is reported in ref 10), but it qualitatively contradicts the experimental observations of Gogotsi et al.[7] and Dujardin et al.[22] However, all of the experimental results might be compromised by contamination of the surface or of the water. A more detailed study of the cases A−B′−C′ reveals that the value of the contact angle has a slight tendency to increase with diameter, but the differences are negligible compared to the estimated errors. Also, the conditional binning seems not to influence the value of the contact angle significantly, the largest difference between case B and its conditionally binned counterpart B′ is 0.6°. The difference between C and C′ is larger, namely 1.2°, which is explained by the high rejection rate of samples in case C′. The contact angle for the conditionally binned cases B′ and C′ are consistently smaller than the ones found for B and C. Together with the observation that the density peaks are larger for the double layer graphite case G_2 than for the single layer graphite case G_1, one expects that the contact angle is likely to be smaller for multiwall CNTs than for the corresponding SWNTs. Also interesting is the comparison between the averaged values of the contact angle for the cases B$^0_+$, B^0, and B$^0_-$, which are 104.8°, 109.5° and 130.8° respectively (averaged over all considered isochores). Even for the case B$^0_+$ with an increased interaction strength, wetting is not observed. The fact that a change in the parameter ϵ_{CO} of ±20% leads to a consistent change in the contact angle suggests that the CNT−water system could be used as a model system for comparison with experiments.

Conclusions. We have conducted parallel molecular dynamics simulations to investigate the wetting behavior of water droplets confined in carbon nanotubes. Contrary to the wetting behavior observed experimentally by Gogotsi et al.[7] and by Dujardin et al.,[22] the present study of pure water in pristine CNT indicates a nonwetting behavior. For the interaction potentials considered, a perturbation of the carbon−water interaction energy of ±20% did not alter the

nonwetting behavior of the interface. We do not expect significant differences in the contact angle for armchair and achiral tubes (the tubes in the present study are all of zigzag type). Small changes could be caused due to a chirality specific mechanical deformation behavior of the CNT and by the electronic structure, which potentially leads to a different carbon water interaction. Direct comparisons of our MD simulations with experimental data would be desirable but are not possible at the present time due to differences in length and time scales as well as discrepancies in the composition of the working materials (impurities). However, the present parallel implementation will soon allow us to approach regimes such as the one probed in the experiments by Gogotsi et al.[7] Further investigations are ongoing to assess the effect of the various terms in the potential functions on the overall wetting behavior of the CNTs. Also, the possible influence of the presence of a pressurized inert gas on the contact angle will be addressed to allow a closer comparison to experiments. We believe that the present results may offer a benchmark study for future experiments of carbon nanotube and water interactions.

References

(1) Iijima, S. *Nature* **1991**, *354*, 56−58.
(2) Hong, M.-H.; Kim, K. H.; Bae, J.; Jhe, W. *Appl. Phys. Lett.* **2000**, *77*(16), 2604−2606.
(3) Noca, F.; Hoenk, M.; Hunt, B.; Koumoutsakos, P.; Walther, J.; Werder, T. *J. Acoust. Soc. Am.* **2000**, *108*(5), 2494.
(4) Ugarte, D.; Stöckli, T.; Bonard, J. M.; Châtelain, A.; de Heer, W. A. *Appl. Phys. A* **1998**, *67*(1), 101−105.
(5) Dujardin, E.; Ebbesen, T. W.; Krishnan, A.; Treacy, M. M. *J. Adv. Mater.* **1998**, *10*(17), 1472−1475.
(6) Gogotsi, Y.; Libera, J. A.; Yoshimura, M. *J. Mater. Res.* **2000**, *15*(12), 2591−2594.
(7) Gogotsi, Y.; Libera, J. A.; Güvenç-Yazicioglu, A.; Megaridis, C. M. *Appl. Phys. Lett.* **2001**, *79*(7), 1021−1023.
(8) Luna, M.; Colchero, J.; Baró, A. M. *J. Phys. Chem. B* **1999**, *103*, 9576−9581.
(9) Gil, A.; Colchero, J.; Luna, M.; Gómez-Herrero, J.; Baró, A. M. *Langmuir* **2000**, *16*, 5086−5092.
(10) Adamson, A. W.; Gast, A. P. *Physical Chemisry of Surfaces*, 6th ed.; John Wiley & Sons: New York, 1997.
(11) Liu, J.; Rinzler, A. G.; Dai, H.; Hafner, J. H.; Bradley, R. K.; Boul, P. J.; Lu, A.; Iverson, T.; Shelimov, K.; Huffman, C. B.; Rodriguez-Macias, F.; Shon, Y.-S.; Lee, T. R.; Colbert, D. T.; Smalley, R. E. *Science* **1998**, *280*, 1253−1256.
(12) Rieutord, F.; Salmeron, M. *J. Phys. Chem. B* **1998**, *102*, 3941−3944.
(13) Gordillo, M. C.; Martí, J. *Chem. Phys. Lett.* **2000**, *329*, 341−345.
(14) Nijmeijer, M. J. P.; Bruin, C.; Bakker, A. F.; van Leeuwen, J. M. J. *Phys. Rev. A* **1990**, *42*(10), 6052−6059.
(15) Teleman, O.; Jönsson, B.; Engström, S. *Mol. Phys.* **1987**, *60*(1), 193−203.
(16) Walther, J. H.; Halicioglu, T.; Jaffe, R.; Koumoutsakos, P. *J. Phys.Chem. B* **2001**, *105*, 9980−9987.
(17) Bojan, M. J.; Vernov, A. V.; Steele, W. A. *Langmuir* **1992**, *8*, 901−908.
(18) Levitt, M.; Hirshberg, M.; Laidig, K. E.; Daggett, V. *J. Phys. Chem. B* **1997**, *101*, 5051−5061.
(19) Berendsen, H. J. C.; Postma, J. P. M.; van Gunsteren, W. F.; DiNola, A.; Haak, J. R. *J. Chem. Phys.* **1984**, *81*(8), 3684−3684.
(20) Martí, J. *Phys. Rev. E* **2000**, *61*(1), 449−456.
(21) Israelachvili, J. N. *Intermolecular and Surface Forces. With Applications to Colloidal and Biological Systems*, 2nd ed.; Academic Press: New York, 1992.
(22) Dujardin, E.; Ebbesen, T. W.; Hiura, H.; Tanigaki, K. *Science* **1994**, *265*, 1850−1852.

NL015640U